Paper published as

On-the-fly outlier rejection in high-precision spaceborne GPS applications

Urbano Tancredi

Dept. of Engineering
University of Naples 'Parthenope'
Naples, Italy
urbano.tancredi@uniparthenope.it

Alfredo Renga and Michele Grassi

Dept. of Industrial Engineering
University of Naples "Federico II"
Naples, Itay
alfredo.renga@unina.it, michele.grassi@unina.it

Abstract—**This paper presents a technique for on-the-fly rejection of GPS pseudorange data outliers. It is developed for applications in whom high accuracy navigation is needed in real time, as for the relative positioning of satellites in Low Earth Orbit. The proposed technique relies on two metrics screening the residual ranging errors in the Zero-Difference and Single-Difference pseudorange measurements with respect to an a-priori threshold. Preliminary tests carried out on flight data from the Gravity Recovery and Climate Experiment mission demonstrate the effectiveness of the proposed approach.**

Keywords—Outlier rejection; Data editing; Global Positioning System; Relative Positioning; Low Earth Orbit

I.   INTRODUCTION

GPS is the ideal sensor for the positioning of satellites flying in Low Earth Orbits (LEO). Both absolute and relative positioning solutions can be achieved and used in a variety of applications, from Earth observation to geodesy and universe science missions. State-of-art dual-frequency receivers and navigation filters achieve decimeter to centimeter positioning accuracy in real-time [1],[2].

However, GPS observables are typically affected by outliers that, if not discovered and effectively rejected, may significantly degrade the positioning solution accuracy [3]. This problem is of particular relevance to applications in which a centimeter-level accuracy is desired.

The present paper focuses on techniques and algorithms for on-the-fly rejection of outliers in pseudorange measurements suitable to autonomous, real-time, onboard relative positioning of formation flying satellites in LEO. Accurate relative navigation of formation flying satellites requires taking into account also the absolute position of one of the satellites. Outlier rejection is thus performed in both absolute or Zero-Difference (ZD) measurements (i.e. measurements collected by each receiver independently) and relative or differenced measurements.

Conventional approaches for outlier rejection in terrestrial applications exploit GPS measurement redundancy [4]. Well-known and widespread RAIM (Receiver Autonomous Integrity Monitoring) techniques are based on this idea. Adaptation of such techniques to spacecraft positioning by GPS is however non-trivial. Very fast spacecraft dynamics (up to 7 km/s), lack of computational resources, and reduced electronics performance due to the harsh space environment are all factors that make this application particularly challenging. Moreover, the orbital altitude degrades the GPS observation geometry, implying that measurement redundancy might not be available for receivers in which the separation (baseline) among the satellites is in the order of hundreds of km. Hence, the present paper is aimed at developing a technique able to perform outlier detection at the current time instant without resorting on GPS measurements at the same time instant. An example of this approach is TurboEdit developed by JPL in the nineties [5],[6] . The method exploits wide-lane and ionospheric free combinations of GPS measurements to detect the outliers epoch-by-epoch based on a polynomial fit of pseudorange measurements. Similar concepts are also used in GPS-based geoscience applications based on different statistical approaches [7]. Concerning GPS applications in LEO, post-processing data editing procedures have been also proposed and successfully tested on real-world GPS data [8]. These methods are, however, of limited practical utility for real-time onboard positioning in LEO. Indeed, they either assume a static receiver or require acquisition of extremely long data arcs, assumptions that do not hold true in these applications.

The paper is organized as follows. Section II illustrates the GPS measurement model and the on-orbit relative geometry. Based on this model, the outlier rejection approach applied to absolute and relative pseudorange measurements is presented in section III. Section IV presents the experimental results achieved by the proposed technique on flight data from the Gravity Recovery and Climate Experiment (GRACE) mission. Finally, Section V draws the conclusions.

II.   MEASUREMENT MODEL

Let us refer to a typical system for Earth observation and geodesy applications [2], comprising two receivers on board two LEO spacecraft, denoted by *Chief* and *Deputy*, separated by a certain baseline **b** (see Fig.1).
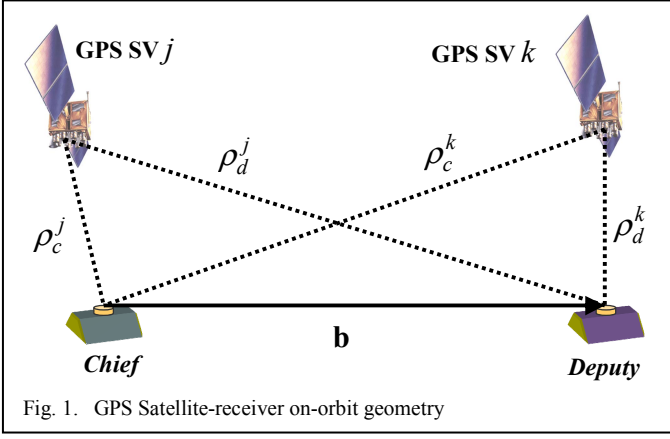
Fig. 1. GPS Satellite-receiver on-orbit geometry

The following standard observation model [9] serves as a basis for relating dual frequency pseudorange GPS observables to the position of the two receivers:

$$\left(P_1\right)_{rec}^{sv} = \left(\rho^*\right)_{rec}^{sv} + i_{rec}^{sv} + \left(\varepsilon_1\right)_{rec}^{sv} \qquad (1a)$$

$$\left(P_2\right)_{rec}^{sv} = \left(\rho^*\right)_{rec}^{sv} + \gamma^{-2} i_{rec}^{sv} + \left(\varepsilon_2\right)_{rec}^{sv} \qquad (1b)$$

where P indicates pseudorange measurements, the subscripts 1 and 2 the L1 and L2 frequency, and sv denotes the GPS Satellite Vehicle (SV) from which the measurement is taken by the receiver rec. The geometric term ρ^* lumps together non-dispersive delays, such as the LoS (Line-of-Sight) distance between the SV sv and the receiver rec ρ_{rec}^{sv}, and the clock biases δt multiplied by the speed of light in vacuum c. The values of the GPS SV clock biases $c\delta t^{sv}$ are estimated using parameters broadcast in the GPS navigation message.

$$\left(\rho^*\right)_{rec}^{sv} = \rho_{rec}^{sv} + c\delta t_{rec} - c\delta t^{sv} \qquad (1c)$$

The first order ionospheric delay on the L1 frequency is denoted as i_{rec}^{sv} and depends on the inverse square of carrier frequency. The ionospheric delay on L2 is thus univocally determined by i_{rec}^{sv} and the ratio between GPS signal wavelengths, $\gamma=\lambda_1/\lambda_2$. At last, the ε terms are assumed mutually uncorrelated Gaussian white noises.

III. PSEUDORANGE OUTLIER REJECTION TECHIQUE

All the tests for pseudorange rejection are based on estimating a residual error conditioned to the measurement under analysis, and compare it with an a-priori threshold C_t. In practice, each test t defines an outlier rejection region out_t, based on a metric $\|f_t\|$ depending on the measurement X_{rec}^{sv}. When the measurement X_{rec}^{sv} is distant by $\|f_t\|$ more than the a-priori threshold from the origin, it is thought to belong to out_t and rejected.

$$out_t := \left\{ X_{rec}^{sv} : \|f_t\|\left(X_{rec}^{sv}\right) > C_t \right\} \qquad (2)$$

The first outlier rejection test screens the residual ranging error in the ZD pseudorange measurements and is thus denoted by the zd subscript. The ionospheric delay term present in the ZD measurement is deleted by forming ionospheric-free combinations [9]. The residual can be then computed once an estimate of the lumped geometric range $\left(\hat{\rho}^*\right)_{rec}^{sv}$ is provided.

$$out_{zd} := \left\{ X_{rec}^{sv} : \|f_{zd}\| > C_{zd} \right\}, \quad C_{zd} = 5 \cdot \sqrt{\text{var}[f_{zd}]} \qquad (3a)$$

$$f_{zd} := \left(P_{IF}\right)_{rec}^{sv} - \left(\hat{\rho}^*\right)_{rec}^{sv} \qquad (3b)$$

$$\left(P_{IF}\right)_{rec}^{sv} = \frac{1}{1-\gamma^2}\left[\left(P_1\right)_{rec}^{sv} - \gamma^2 \left(P_2\right)_{rec}^{sv}\right] \qquad (3c)$$

The a-priori outlier rejection threshold C_{zd} is fixed as five times the expected standard deviation of the f_{zd} indicator function. The five-sigma bound has been fixed for rejecting large errors while still being capable of using as much as observations as possible in the unfavorable GPS observation geometry from LEO.

The second outlier rejection test applies the same metric of Eq.(3) to Single-Difference (SD) pseudorange measurements, thus it is denoted by the sd subscript. The f_{sd} indicator function is taken as the SD of the f_{zd} ones for the chief and deputy receivers, whose relevant variables are denoted by the c and d subscript, respectively. Hence, introducing the SD operator as $\Delta_d(\cdot) = (\cdot)_d - (\cdot)_c$, the f_{sd} function can be written as

$$\left(f_{sd}\right)^{sv} = \Delta_{dc}\left(f_{zd}\right)^{sv} =$$
$$= \left(P_{IF}\right)_d^{sv} - \left(P_{IF}\right)_c^{sv} - \left(\hat{\rho}^*\right)_d^{sv} + \left(\hat{\rho}^*\right)_c^{sv} \qquad (4a)$$

Also in this case, the residual can be computed once an estimate of the SD geometric term is provided. Being the f_{sd} metric based on SD measurements, if a measurement is classified as an outlier for one receiver, it will be classified as an outlier for the other receiver as well. It is worth noting that measurements of GPS satellites not in common view of the two receivers cannot be screened by such test. The a-priori outlier rejection threshold C_{sd} is fixed to the five-sigma bound in this case as well. The outlier rejection region is thus expressed as follows.

$$out_{sd} := \left\{ X_{rec}^{sv} : \left(f_{sd}\right)^{sv} > C_{sd} \right\}, \quad C_{sd} = 5 \cdot \sqrt{\text{var}[f_{sd}]} \qquad (4b)$$

In order to perform the above tests on the fly, the relevant geometric and clock terms must be estimated in real-time. This requires computing the receiver position and clock bias at any time t_k without resorting to the GPS measurements at the same time instant. Hence, an extrapolation from time t_{k-1} is needed. To this end, the correlation in time of each receiver's position (caused by the orbital dynamics) and clock bias is exploited. In this respect, these estimates are obtained in real-time as the result of the propagation step of an EKF (Extended Kalman Filter), as shown in Fig.2. Details about the EKF formulations used, whose accuracy is compatible with the previously

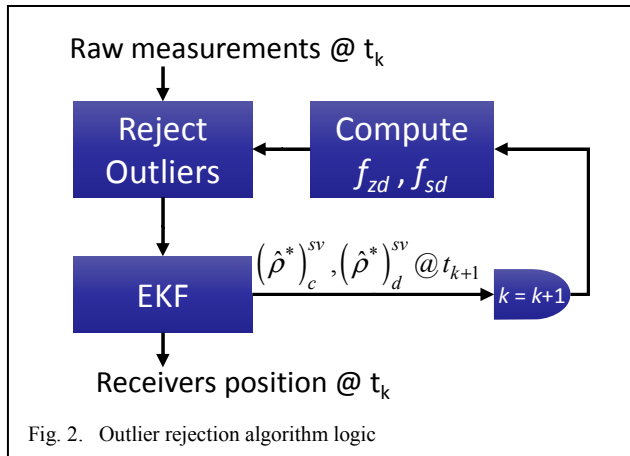introduced outlier indicator functions, can be found in [2],[10],[11].

Fig. 2.   Outlier rejection algorithm logic

The outlier rejection thresholds are fixed a-priori, i.e. without looking at the f functions realizations on the measured data. This allows avoiding potentially unstable feedback loops between the data screened and the pruning indicator functions. Instead, a constant a-priori variance is specified for both pseudorange measurements and the lumped geometric term as estimated by the EKF, obtaining an estimate of the rejection threshold by consequence.

Denote by σ_i the standard deviations of the P_i measurement noises and by σ_ρ the lumped geometric term one. Pseudorange measurements on L1 and L2 can be considered mutually uncorrelated [12]. The lumped geometric term is also assumed uncorrelated with the measurements. Indeed, it is computed without resorting to the GPS measurements at the same time instant. The variance of the f_{zd} function is thus estimated by

$$\mathrm{var}\left[f_{zd}\right] \cong \frac{1}{\left(1-\gamma^2\right)^2}\left[\sigma_1^2 + \gamma^4 \sigma_2^2\right] + \sigma_\rho^2 \qquad (5a)$$

The variance of the f_{sd} function is estimated under the same assumptions of the ZD case and modelling the correlation among variables relevant to different receivers. The white pseudorange measurement noises ε are uncorrelated between the two receivers. Correlation of the lumped geometric term between the receivers is instead taken into account. Indeed, ρ^* is estimated using GPS measurements up to time t_{k-1} (Fig.2), which are correlated in space. For receivers separated by a distance in the order of kilometers, differential GPS (i.e. removing errors in common between receivers) is capable of reducing the ranging error of one order of magnitude. The f_{zd} function's variance is thus modeled as follows, where the correlation between the lumped ranges of the two receivers acts as an additional parameter.

$$\mathrm{var}\left[f_{sd}\right] = 2\left\{\mathrm{var}\left[f_{zd}\right] - \sigma_\rho^2 \cdot \mathrm{corr}\left[\left(\hat{\rho}^*\right)_d^{sv}, \left(\hat{\rho}^*\right)_c^{sv}\right]\right\} \qquad (5b)$$

IV.   TEST RESULTS

The proposed algorithm has been tested on real-world data from the GRACE mission, launched in 2002, consisting of two identical satellites, GRACE A and GRACE B, flying in tandem with a nominal separation of 220 km, in near circular orbits at an initial altitude of approximately 500 km and 89.5 deg inclination [13]. The two satellites have two identical NASA JPL BlackJack GPS receivers [14]. A post-processed version of the GRACE data, known as Level 1B (L1B) data, is available to the scientific community by JPL's Physical Oceanography Distributed Active Archive Center (PODAAC). The Level 1B data are derived from the processing applied to the raw data described by [15]. GPS data used in this paper consist of pseudorange and carrier phase measurements from code observations on the L1 frequency and semi-codeless tracking on the L2 frequency. Data time-tags are corrected to GPS time using GPS clock solutions computed in post-processing [16]. Performance of the proposed technique is quantified by using the GPS Navigation (GNV) Level 1B data product, which contains an estimate of the two spacecraft Center of Mass (CoM) position vectors with a time-varying accuracy of a few centimeters [15]. The data set selected for this analysis refers to October 22nd 2011, which is representative of the most intense ionospheric conditions across the overall GRACE data set from 2005 to June 2013. The values used for a-priori modeling of the measurements and lumped range have been fixed taking into account the typical performance of NASA JPL BlackJack GPS receivers and of the used EKF formulation. The correlation between the lumped ranges depends upon the distance between receivers, with unit values for nearby receivers. Because of the O(200 km) distance between the two receivers, a positive 60% correlation has been enforced. Table 1 lists all the fixed parameters, as well as the resulting outliers rejection thresholds.

Fig. 3 and 4 show the time profile of the ZD (for the chief receiver) and SD pseudorange outlier indicator functions as computed by the real-time algorithm, i.e. using broadcast ephemerides and the EKF predictions to compensate the geometric terms in Eq.s (3),(4). Pseudorange measurements determining values in the two metrics well above the threshold are clearly visible, and are rejected on the fly by the data editing process.

TABLE I.   PARAMETERS FOR OUTLIERS REJECTION THRESHOLDS

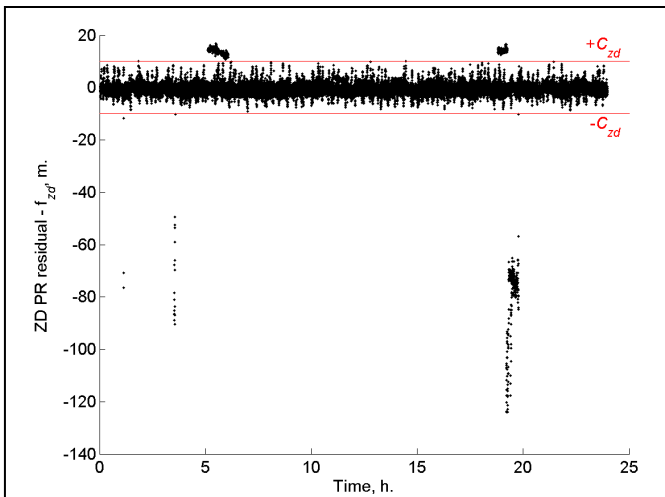| Variable	Value
σ_1	20 cm
σ_2	25 cm
σ_ρ	200 cm
$\mathrm{corr}[(\rho^*)_d, (\rho^*)_c]$	0.60
C_{zd}	10.50 m
C_{sd}	10.02 m

Fig. 3. Computed ZD PR outlier indicator function for raw measurements – chief spacecraft
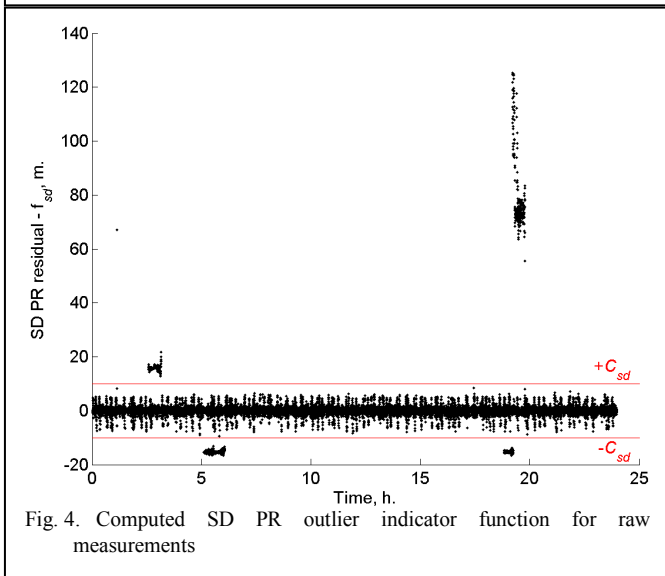

Fig. 4. Computed SD PR outlier indicator function for raw measurements

In order to evaluate the effectiveness of the data pruning, its effect on the positioning error is analyzed. A single-epoch kinematic position fix is obtained using pseudoranges before and after the outlier rejection. Fig. 5 and 6 show the errors in the chief's absolute position before and after outlier rejection. Similar results hold for deputy receiver and are not shown for brevity.

Residual position errors are projected in the Orbiting Reference Frame, customarily employed in formation flying and remote sensing applications. This reference frame, shown in Fig.7, identifies the cross track direction, i.e. the normal to the orbital plane in the direction of the angular momentum, the radial direction, opposite to the chief's spacecraft position vector, and the along track direction to form a Cartesian reference frame.

Results suggest that the projected algorithm is capable of reducing the positioning error r.m.s. value of a factor of 4, confirming its effectiveness.

At last, an assessment of the accuracy with whom the lumped geometric term can be estimated in real time is presented to gain further insight on the performance of the proposed algorithm. Fig. 8 shows the difference between the ZD and SD geometry terms predicted by the EKF and used by the data-editing algorithm versus their *true* values as computed by GNV data. The ZD and SD geometry can be estimated with meter and decimeter-level accuracy, respectively, which compares well with the selected thresholds for outlier rejection.
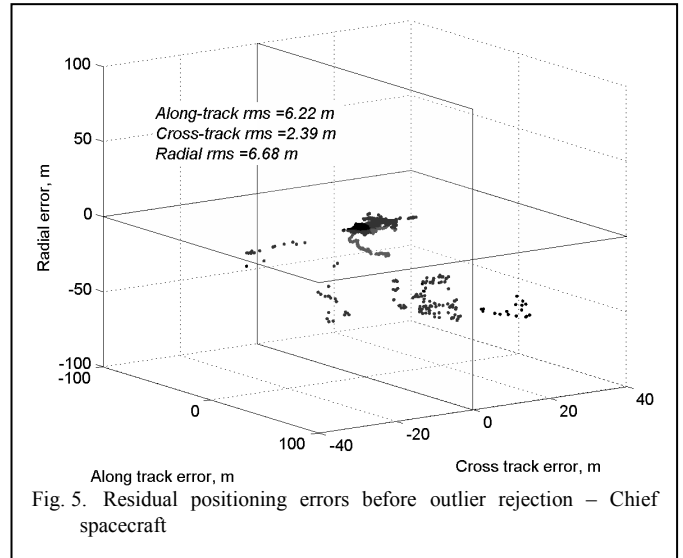

Fig. 5. Residual positioning errors before outlier rejection – Chief spacecraft
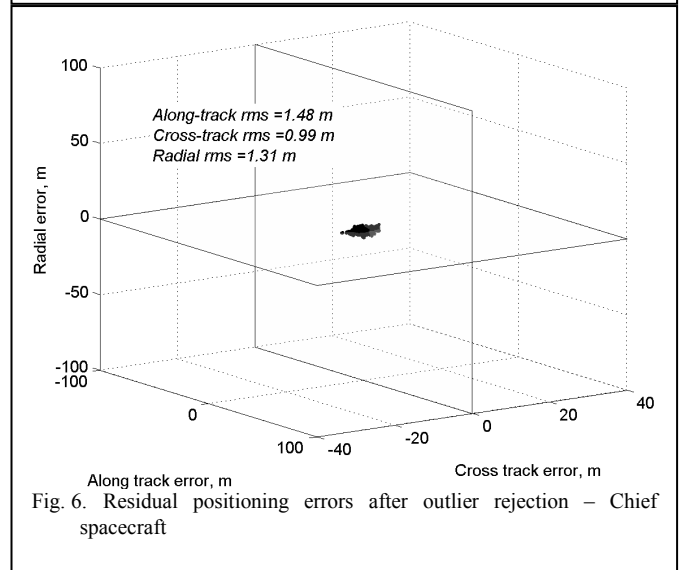

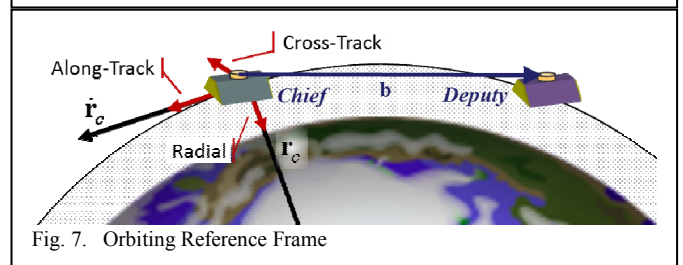Fig. 6. Residual positioning errors after outlier rejection – Chief spacecraft
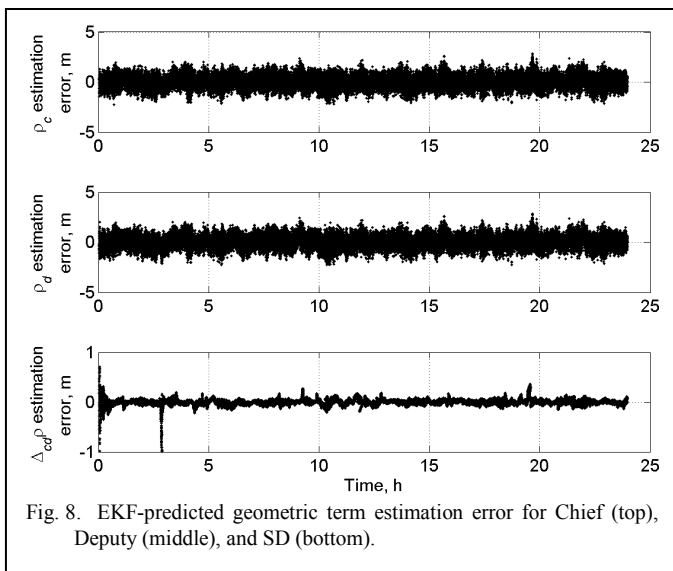

Fig. 7. Orbiting Reference Frame

Fig. 8. EKF-predicted geometric term estimation error for Chief (top), Deputy (middle), and SD (bottom).

V. CONCLUSION

This paper has described a technique for on-the-fly rejection of GPS data outliers that may significantly degrade the positioning accuracy of receivers flying in LEO. The presented technique relies on two metrics that screen the residual ranging errors in the ZD and SD pseudorange measurements with respect to prefixed thresholds. These metrics are computed in real-time by providing ZD and SD geometric range estimates through state-of-art navigation filters available on LEO satellites.

The effectiveness of the proposed technique has been tested on true world flight data from the Gravity Recovery And Climate Experiment, consisting of two spacecraft flying in tandem with a nominal separation of 220 km. For this mission, both GPS receiver measurements and high-accuracy orbital data products are made available to the international scientific community. Results prove that the proposed technique can actually reject all the pseudorange outliers identified in the available data set. Future activities will be concerned with carrier-phase outlier identification and rejection.

REFERENCES

[1] O. Montenbruck, S. D'Amico, GPS Based Relative Navigation,, in M. D'Errico (ed.) Distributed Space Missions for Earth System Monitoring, Space Technology Library, 2013, Vol. 31, Part II, pp. 185-224..

[2] U.Tancredi et al, "Real-time relative positioning of spacecraft over long baselines", AIAA Journal of Guidance, Control and Dynamics, Vol. 37, No.1, Jan.-Feb. 2014

[3] O. Montenbruck, R. Kroes, "In-flight performance analysis of the CHAMP BlackJack GPS Receiver", GPS Solutions, Vol. 7, No. 2, pp. 74-86, 2003.

[4] UnderstandingvGPS—Principles and Applications, E. D. Kaplan and C. J. Hegarty, Eds., Artech House, London, UK, 2nd edition, 2006-

[5] G. Blewitt, "An Automatic Editing Algorithm for GPS Data", Geophysical Research Letters, VOl. 17, No. 3, pp. 199-202, 1990.

[6] G. Blewitt, "GPS data processing methodology: from theory to applications", GPS for Geodesy, ch. 6, p. 231-270, Springer-Verlag, Berlin, 1998.

[7] Guochang Xu, "GPS: Theory, Algorithms and Applications", 2 Edition, Springer-Verlag, Berlin, 2007.

[8] R. Kroes, "Precise Relative Positioning of Formation Flying Spacecraft using GPS", Ph.D. Thesis, Delft Univ. of Technology, Delft, The Netherlands, 2006.

[9] J. A. Farrell, Aided Navigation: GPS with high rate sensors, McGraw-Hill, New York, 2008

[10] S. D'Amico, et al, "Spaceborne Autonomous Formation-Flying Experiment on the PRISMA Mission", AIAA Journal of Guidance, Control and Dynamics, Vol. 35, No. 3 (2012), pp. 834-850, doi: 10.2514/1.55638.

[11] S. D'Amico et al, "Autonomous formation flying based on GPS - PRISMA flight results", Acta Astronautica, Vol. 82, No.1, Jan. 2013, Pages 69–79.

[12] Bona, P. 'Precision, Cross Correlation, and Time Correlation of GPS Phase and Code Observations', *GPS Solutions* Vol. 4, No. (2), 2000, p.3-13.

[13] Tapley, B. D., Bettadpur, S., Watkins, M., Reigber, C., , Geophys. Res. Lett., Vol. 31, No. 9, L09607, 10.1029/2004GL019920, 08 May 2004. Copyright 2004, American Geophysical Union.

[14] G. Davis, E. Davis, S. Luthcke, K. Hawkins, Pre-Launch Testing of GPS Receivers for Geodetic Space Missions, in: Proceedings of the 13th International Technical Meeting of the Satellite Division of The Institute of Navigation, Salt Lake City, USA, 2000, pp. 2009–2018.

[15] S.C. Wu, G. Kruizinga, W. Bertiger, Algorithm theoretical basis document for GRACE level 1B data processing, NASA Jet Propulsion, Laboratory, revision 1.2, JPL D-27672, GRACE 327-741, 2006

[16] K. Case, G. Kruizinga, S.C. Wu, GRACE level 1B data product user handbook, NASA Jet Propulsion Laboratory, revision 1.3, JPL D-22027, GRACE 327-733, 2010